Original Research

Tumor Immunity Microenvironment-based classifications of bladder cancer for enhancing cancer immunotherapy

Jialin Meng[1#], Xiaofan Lu[2#], Yujie Zhou[3#], Meng Zhang[1,4], Jun Zhou[1], Zongyao Hao[1], Yinan Du[5], Fangrong Yan[2*], Chaozhao Liang[1*]

1. Department of Urology, The First Affiliated Hospital of Anhui Medical University; Institute of Urology & Anhui Province Key Laboratory of Genitourinary Diseases, Anhui Medical University, Hefei, 230022, P.R. China.
2. State Key Laboratory of Natural Medicines, Research Center of Biostatistics and Computational Pharmacy, China Pharmaceutical University, Nanjing 211198, P.R. China.
3. Division of Gastroenterology and Hepatology, Key Laboratory of Gastroenterology and Hepatology, Ministry of Health, Renji Hospital, School of Medicine, Shanghai Jiao Tong University, Shanghai Institute of Digestive Disease, Shanghai, 200127, P.R. China.
4. Urology Institute of Shenzhen University, The Third Affiliated Hospital of Shenzhen University, Shenzhen University, Shenzhen, 518000, P.R. China.
5. School of Basic Medical Sciences, Anhui Medical University, Hefei, Anhui 230032, P.R. China.

# These authors contributed equally to the study.

*__Correspondence:__

Prof. Fangrong Yan

State Key Laboratory of Natural Medicines, Research Center of Biostatistics and Computational Pharmacy, China Pharmaceutical University

Nanjing 211198, P.R. China.

f.r.yan@163.com

Prof. Chaozhao Liang

Department of Urology, The First Affiliated Hospital of Anhui Medical University; Institute of Urology & Anhui Province Key Laboratory of Genitourinary Diseases, Anhui Medical University

218th Jixi Road, Hefei, 230022, P.R. China

liang_chaozhao@ahmu.edu.cn

Running title: Immune classifications of bladder cancer for immunotherapy

ABSTRACT

Background: Bladder cancer is composed by a mass of heterogenetic characteristics, immunotherapy is a potential way to save the life of bladder cancer patients, but only benefit to about 20% patients.

Methods and materials: A total of 4003 bladder cancer patients from 19 cohorts was enrolled in this study, collecting the clinical information and mRNA expression profile. The unsupervised non-negative matrix factorization (NMF) and nearest template prediction (NTP) algorithm was used to divide the patients to immune activated, immune exhausted and non-immune class. Verified gene sets of signatures were used to illustrate the characteristic of immunophenotypes. Clinical and genetic features were compared in different immunophenotypes.

Results: We identified the immune class and non-immune classes in from TCGA-BLCA cohort. The 150 top different expression genes between these two classes was extracted as the input profile for the reappearing of the classification in the other 19 cohorts. As to the activated and exhausted subgroups, a stromal activation signature was conducted by NTP algorithm. Patients in the immune classes shown the highly enriched signatures of immunocytes, while the exhausted subgroup also shown an increased signature of TITR, WNT/TGF-β, TGF-β1 activated, and C-ECM signatures. Patients in the immune activated shown a lower CNA burden, better overall survival, and favorable response to anti-PD-1 therapy.

Conclusion: We defined and validated a novel classifier among the 4003 bladder cancer patients. Anti-PD-1 immunotherapy could benefit more for the patients belong to immune activated subgroup, while ICB therapy plus TGF-β inhibitor or EP300 inhibitor might be more effectiveness for patients in immune exhausted subgroup.

Keywords: bladder cancer, non-negative matrix factorization, immunotherapy, immune checkpoints blockade

INTRODUCTION

Bladder cancer is the 10th most frequent tumor globally, of which with a high rate of recurrence[1]. There are about 550 thousand new cases and 200 thousand specific deaths caused by bladder cancer each year. The incidence rate of bladder cancer variable around the world, with the highest rate in Southern Europe, and lowest rate at Middle Africa[2]. In United States, bladder cancer ranges the 6th common tumor, with about 81 thousand new cases and 18 thousand new deaths at 2020[3]. Most patients diagnosed at the early stage of bladder cancer, also known as the non-muscle-invasive bladder cancer (NMIBC), which only processes away from the muscle layer and could be removed easily through the transurethral resection (TUR), or plus with the intravesical therapy with Bacillus Calmette-Guérin (BCG) or other chemotherapeutic medicine [4-6]. Recurrence is extremely common in NMIBC, about 70% patients will suffer from the health burden of bladder cancer again within 10 years, and one thirds of them step into advanced stage, also called muscle-invasive bladder cancer (MIBC)[7]. The standard care of MIBC is radical cystectomy with or without neoadjuvant chemotherapy or chemoradiation. And even after the treatment, almost 50% MIBC patients will recurrent and death from the metastatic stage within 3 years[8].

In the tumor mass, the normal cells, blood vessels, and cytokines which surround and support the alive of tumor cells are composes of the tumor microenvironmnt (TIME). The cross talk existed between the tumor and the TIME, the tumor cells could alter the TIME, and the TIME could also promote the growth and spread of the tumors[9]. Several studies investigated the diagnosis markers, prognostic signatures or therapeutic targets for

93 malignancy tumors based on the TIME, as well as in bladder cancer. BCG is the earliest
94 immune therapy approved in bladder cancer treatment, which could stimulate an
95 immunologic reaction inducing a proinflammatory cytokine and direct cell-to-cell
96 cytotoxicity[10]. BCG is still the standard therapy for NMIBC, which reflect that bladder
97 cancer patients could benefit from immunotherapy. The development of the blockade of
98 immune checkpoints also applied in the treatment of bladder cancer. Two PD-1 inhibitors
99 (pembrolizumab and nivolumab) and three PD-L1 inhibitors (atezolizumab, durvalumab,
100 and avelumab) were approved by the FDA for the treatment of bladder cancer
101 (https://www.accessdata.fda.gov/scripts/cder/daf). In the IMvigor210 clinical study,
102 atezolizumab was used to block the PD-L1, the objective response rate (ORR) for
103 IMvigor210 cohort 1 is only 23%, 15% in the cohort 2[11,12]. The ORR for Nivolumab and
104 durvalumab is similar, from 17% to 24.4%[13-16]. Therefore, a full understanding of the
105 immunophenotypes to bladder cancer is essential, which could as the guidance to choose
106 the patients to receive the appropriate immunotherapy.

107 We enrolled 4003 bladder cancer patients from 20 independent cohorts. Non-negative
108 matrix factorization (NMF) algorithm and nearest template prediction (NTP) was applied
109 to distinguish the immunophenotypes of bladder cancer patients in training cohort of
110 TCGA-BLCA, as well as validated in the other 19 cohorts. The novel definition of
111 immunophenotypes could provide illuminations for the immunotherapy of bladder cancer
112 patients.

113

114 **MATERIALS AND METHODS**

115 **Bladder cancer patient cohorts**

4003 bladder cancer patients were registered in the current study, with the gene expression profiles, clinicopathological information and overall survival data (**Figure 1**). For TCGA-BLCA cohort, we obtained the level 3 gene expression profile of 408 patients from TCGA Data Portal (https://tcga-data.nci.nih.gov/tcga), only genes expressed in at least 50% of the samples were retained for analyses. For the further external validation cohorts, GSE32894, GSE83586, GSE87304, GSE128702, GSE13507, GSE129871, GSE120736, GSE39016, GSE128701, GSE124035, GSE86411, GSE48276, GSE31684, GSE134292, GSE69795, the gene expression profile were collected from Gene Expression Omnibus (http://www.ncbi.nlm.nih.gov/geo/). For E-MTAB-4321 and E-MTAB-1803 cohorts, the gene expression profile were downloaded from ArrayExpress (https://www.ebi.ac.uk/arrayexpress/). For IMvigor210 cohort, the gene expression profile was obtained from IMvigor210CoreBiologies, a data package for the R statistical computing environment. Detailed information of these datasets was displayed in **Table S1.**

Bioinformatic analyses

The mRNA expression profile of 408 bladder cancer patients from TCGA-BLCA cohort were microdissected by the unsupervised non-negative matrix factorization (NMF) algorithm[17]. Immune module was selected with the gathering of patients with the high immune enrichment score calculated by the the single-sample gene set enrichment analysis (ssGSEA) as described previously[18]. Top 150 exemplar genes with the highest weight in the immune module was extracted as the key genes to dichotomize the immune and non-immune classes, which further modified by the multidimensional scaling random forest method[19]. Immune activated and exhausted subgroups were recognized by the stromal activation signature with nearest template prediction[20]. To depict the characteristics of these three immunophenotypes, several immune associated signatures were manually collected and the score of each signature for each patient were generated

via ssGSEA (**Table S2**). The different genetic types among immune and non-immune classes were evaluated, including tumor-infiltrating lymphocytes (TILs) abundance, Programmed death-ligand 1 (PD-L1) expression, Copy number alterations (CNA), tumor mutation burden (TMB), neoantigens and mutant genes. To reappearing the immunophenotypes we generated, the expression profile of the top 150 differentially expressed genes (DEGs), which increased in immune class than non-immune class, were used to dichotomize the immune classes in validation cohorts with the NMFConsensus method, immune class divided into activated and exhausted subgroups subsequently. Details about the enrolled cohosts, as well as the specific method of each step were provided in the **Supplementary Materials and Methods**.

RESULTS

Identify the immune module and derivate immune class of bladder cancer

We performed the virtual microdissection with the NMF algorithm, the mRNA expression profile of 408 bladder cancer patients from TCGA-BLCA cohort was analyzed as the training cohort. To obtain the robust immune module, we pre-set the numbers of module as five to 10, respectively, finally, when the total modules is nine, the first module strongly enriched the patients with a highly immune enrichment score (IES), of which defined as the immune module (**Figure 2A**). The top 150 weighted genes in the immune module were defined as the exemplar genes which could inflect the characteristics of the immune module (**Table S3**). These genes were involved in the signaling pathways of T cell activation, antigen processing and presentation, B cell activation based on the analysis among ontology biological process, and associated with the activation of the pathways related with Th1/Th2 cell differentiation, T cell receptor signaling pathway, B cell receptor

signaling pathway, and PD-L1 expression/PD-1 checkpoint pathway (all, $P < 0.05$, **Table S4**). Subsequently, we re-defined the total 408 bladder patients to immune enriched or non-immune enriched groups by the consensus clustering based on the 150 exemplar genes (**Figure 2B**), what's more, the multidimensional scaling (MDS) random forest was further employed to define a more precise classify of immune and non-immune classes (**Figure 2C**). In **Figure 2D**, the distribution and association of the 408 bladder cancer patients among NMF modules, immune module weight, exemplar gene clustering, final immune classes and immune enrichment score was shown.

Several immune associated signatures (**Table S2**) were collected to help us to confirm the classification of immune or non-immune classes, the enrichment score of each signature among each patient were conducted by ssGSEA. We observed the increased enrichment of T cells (reflected by the signatures of 13 T-cell signature, T cells, CD8+ T cells, T. NK. Metagene), B cells (reflected by the signatures of B-cell cluster, B.P. meta), macrophages, tertiary lymphoid structure (TLS), cytolytic activity score (CYT) and IFN signatures (all, $P < 0.05$, **Figure 3**). We also analyzed the activated KEGG signaling pathways by GSEA, we revealed that the immune cell pathways (including T cell, B cell, natural killer cell and leukocyte associated pathways), immune response pathways (including chemokine signaling pathways, antigen processing presentation, cell adhesion molecules cams and complement coagulation cascades), proinflammatory pathways (including FC-Epsilon-RI, NOD like receptor and FC gamma R mediated phagocytosis pathways) were all active in the immune class (**Figure S1**). Taken together the results from **Figure 2**, **Figure 3 up panel, Figure S1**, and **Table S3-S4**, we microdissected the immune and non-immune classes in TCGA-BLCA cohort, activated immune associated signatures and signaling pathways were observed in the immune class.

Tumor immune microenvironment to immunophenotypes distinguished by activation of stromal cells

Fibroblasts, mesenchymal stromal cells (MSCs), and extracellular matrix (ECM) are the key components to compose the tumor stroma, support and connective the tumor cells[21]. Especially at the late stage of tumors, the genetic and epigenetic alterations of the tumor cells were driven by the activated stroma components[22]. MSCs act as the inherently regulators of tumor, which could secreta the inhibiting soluble factors and alter the cell surface markers to suppress the immune microenvironment, the inhibition of T-cell proliferation and induction of T regulatory cells (Tregs) were all affected by the regulation of PD-L1 by MSCs[23,24]. MSCs could handle the function of suppress immune process through decreasing the expression of pro-inflammatory factors, including IFN-γ, TNF-α and IL-1β, or promoting the expression of type 2 factors, IL-10 and IL13[25,26 27]. For this reason, the previously defined stromal activated signature was employed to further divide the immune class to immune activated and exhausted immunophenotypes, which could reflect the immune response status. A total of 11.0% (45/408) bladder cancer patients in TCGA-BLCA cohort was defined with the activated immunophenotype and inactivated stromal phenotype, belong to immune activated subgroup, while the other 27.0% (110/408) patients belong to immune exhausted subgroup, with the activated stromal phenotype (**Figure 3**). The ECM cytokines (C-ECM) secreted by the fibroblasts could recruit the immunosuppressive cells, the TGF-β is an accepted immunosuppressor in the immune microenvironment, as well as the Treg cells and MDSC cells could reflect the immune exhausted status in TME[28-31]. These signatures were evaluated by ssGSEA analysis, and we revealed that the TITR, WNT/TGF-β, TGF-β1 activated, and C-ECM signatures were higher in the immune exhausted subgroup than activated subgroup (all, $P < 0.05$, **Figure 3, Figure S2**). TIM-3 and LAG3 are reported associated with the immune exhausted

status[32,33], we also generated the similar results in the immune activated and immune exhausted subgroups, increased TIM-3 (P = 0.008) and LAG3 (P = 0.218) were observed in the immune exhausted subgroup (**Figure S2**). Based on the results from **Figure 3 down panel** and **Figure S2**, we separated the immune class into immune activated and immune exhausted subgroups, stromal enrichment score, TITR, MDSC and WNT/TGF-β signatures increased in the immune exhausted subgroup, and also validated by the immune exhausted markers, TIM-3 and LAG3.

The heterogeneity of genetic phenotypes among immune and non-immune classes

To confirm the infiltration of immunocytes among the immune and non-immune classes distinguished by the mRNA expression profile of the exemplar genes, we compared the tumor-infiltrating lymphocytes (TIL) abundance of the 408 bladder cancer patients, which was anteriorly estimated by the Hematoxylin-eosin staining (H&E) stained whole-slide images of TCGA samples[34]. We obtained the result that the TIL abundance is higher in the immune class than non-immune class (P < 0.001, **Figure 4A**), consistent with the definition of these two groups. What's more, we also observed the high expressed PD-L1 level in the immune class than non-immune class (P < 0.001, **Figure 4B**). The gene copy number alteration (CNA), tumor mutant burden (TMB), and neoantigens was reported have the crosstalk with tumor immune activation. Patients in the non-immune class shown an increased level of deletion in both arm and focal level ($P_{\text{Arm-del}}$ < 0.001, $P_{\text{Focal-del}}$ = 0.007), but not the CNA amplification ($P_{\text{Arm-Amp}}$ = 0.733, and $P_{\text{Focal-Amp}}$ = 0.065) (**Figure 4C**), which reflected the positive association of immune infiltration and gene CNA deletion. With the online tool of TIMER, we double confirmed the association between immune infiltration and gene CNA deletion, the deep deletion and arm-level deletion of PD-1, PD-L1 and CTLA4, the three major immune checkpoints, linked with the decreased immunocytes infiltration, especially for CD4+ T cell, Neutrophil, and dendritic cell (**Figure S3)**.

The TMB in immune class is higher than that in non-immune class (P = 0.01, **Figure 4D**), while the neoantigens level shown no difference (P = 0.109, **Figure 4E**). We further compared the specific gene mutations in the immune subgroups (**Figure 4F**). The mutation of TP53 (53.5% vs. 43.1%, P = 0.051), TTN (52.9% vs. 39.5%, P = 0.011), PIK3CA (28.0% vs. 17.0%, P = 0.007) and RB1 (26.0% vs. 13.0%, P < 0.001) appeared more in the immune class than non-immune class (**Figure 5A**). While ERBB2 (P = 0.035), KMT2A (P = 0.013), PKHD1 (P = 0.007) and MDN1 (P = 0.015) similar to be the specific mutations of immune activated subgroup(**Figure 5B**), and EP300 (P = 0.020), HMCN1 (P = 0.014), AKAP9 (P = 0.003) and MACF1 (P = 0.016) mutant patients enriched more in immune exhausted subgroups(**Figure 5C**). Taken together the results from **Figure 4**, **Figure 5**, and **Figure S3**, our results reveal that the immune class is correlated with significantly lower copy number deletion, higher TILs abundance, higher TMB, higher PD-L1, but not neoantigens. The specific mutant genes in the immunophenotypes are diverse.

Reappearing the three immunophenotypes in 19 external cohorts

19 external cohorts with the mRNA expression profile were collected to reappear the three immunophenotypes defined by the NMF algorithm microdissected and activated stroma signature (**Figure 1, Table S1**). The increased top 150 different expression genes (DEGs) between the immune and non-immune classes (**Table S5**) was chosen as the seed genes to reappear the immune subclasses in the external cohorts with the GenePattern module “NMFConsensus”, and then, the immune class divided to activated and exhausted subgroups by the and nearest template prediction (NTP) module.

In GSE32894 cohort, 60.7% (187/308) patients identified as the non-immune class, with the lower enrichment of immune associated signatures, as for the remaining 121 patients, compared with the signatures of stromal enrichment, 42 patients belong to the immune

264 activated subgroup, and 79 belong to the immune exhausted subgroup. Patients in the
265 immune exhausted subgroup shown a high enrichment score of TITR, MDSC, WNT/TGFβ,
266 TGFβ-1 activated and C-ECM signatures (all, $P < 0.01$, **Figure 6**).

267 In the other 3287 bladder cancer patients from 18 cohorts, we also reappeared the three
268 immunophenotypes, the results displayed in **Figure S4** to **Figure 21**. In these cohorts, the
269 distribution of immune activated subgroups ranged from 11.3% to 30.9%, while the
270 proportion of immune exhausted subgroups ranged from 17.1% to 40.8%. We also
271 observed the increased scores of immune enrichment signature and immune signaling
272 signature in the 18 validation cohorts, as well as the other immunocytes signatures. As
273 expected, the subgroup of immune exhausted shown an increased enrichment score of
274 Treg cells, TITR, MDSC, WNT/TGFβ, and C-ECM signatures. Taken together, combined
275 results from **Table S5, Figure 6, and Figure S4 to S21**, our results suggest that the NMF
276 and NTP algorithms could stably and precisely divide bladder patients into immune
277 activated, immune exhausted and non-immune phenotypes. The specific immune
278 characteristics could reappearing in any bladder cancer patients cohort.

279 **Immune activated subgroup shows favorable prognosis and benefits more from**
280 **anti-PD-1 therapy**

281 We collected the overall survival status and time form the TCGA-BLCA, GSE32894,
282 GSE13507 and E-MTAB-1803 cohorts. The prognosis of patients in the three
283 immunophenotypes are dramatically difference. In TCGA-BLCA cohort, we observed the
284 best OS outcome in immune activated subgroup among patients older than 70 years old,
285 while the survival plots of immune exhausted subgroup and non-immune class mixed
286 (**Figure 7A**, $P = 0.45$). What's more, the prognosis obviously distinguished between the
287 three immunophenotypes in GSE32894 cohort (**Figure 7A**, $P < 0.001$). Patients in the

immune activated subgroup all alive at the end of follow-up, patients belong to the non-immune class shown a low rate of death, 5.96% (9/151), while about one thirds patients (16/47) in the immune exhausted subgroup met the death end. The similar tendency of better prognosis in immune activated subgroup, worse prognosis in immune exhausted subgroup was also observed in E-MTAB-1803 cohort and GSE13507 cohort (**Figure 7A**).

Subsequently, we predict the potential response to anti-PD-1 and CTAL4 therapy of the patients in difference immunophenotypes. The module of SubMap in GenePattern was employed to compare the similarity of gene expression profile between the immunophenotypes and responders of anti-CTLA-4 or anti-PD-1 in the metastatic melanoma immunotherapy cohort. We successfully generated the results that patients in the immune activated subgroups could benefit more from the treatment of anti-PD-1 therapy but not anti-CTLA-4 therapy in TCGA-BLCA, GSE32894, and E-MTAB-1803 cohorts (Bonferroni-corrected $P < 0.05$, **Figure 7B**). Taken together of the results from **Figure 7,** we generated the conclusion of that patients in the immune activated subgroup have the longest average overall survival and could benefit more from the anti-PD-1 therapy.

Correlate three immunophenotypes with proposed molecular subtypes

We also sought to integrate the immunophenotypes with the prior established immune molecular features. Thorsson *et al.*[35] generated a six-subtype immune molecular feature, including wound healing (C1), IFN-γ dominant (C2), inflammatory (C3), lymphocyte depleted (C4), immunologically quiet (C5), and TGF-β dominant (C6). We found that most patients in the immune activated subgroup (75.00%) belong to the IFN-γ group, which associated with a strong CD8 signal and a high proliferation rate, and about 68.22% patients in the immune exhausted subgroup also belong to the IFN- γ group (**Figure 8A**).

Kamoun et al.[36] identified a consensus set of six molecular classes: luminal papillary (24%), luminal nonspecified (8%), luminal unstable (15%), stroma-rich (15%), basal/squamous (35%), and neuroendocrine-like (3%). In the current study, we revealed that most immune exhausted patients and half of immune activated patients belong to the basal/squamous classes (**Figure 8B**), which with the most frequently mutated genes of TP53, consistent with what we generated previously (**Figure 5A**). Unquestionably, the Ba/sq subclass associated with the poor prognosis, and patients in the immune exhausted subgroup also shown the poor prognosis.

DISCUSSION

Bladder cancer is a heavy health burden all over the world, especially at Europe and Northern America[2]. The major challenge of bladder cancer clinical care is the short-term recurrence of NMIBC, as well as the shorten overall survival of MIBC patients, especially for those with distant metastases, with the 5-year survival rate less than 10%[7,37]. Iridates from the molecular side, bladder cancer is composed by a mass of heterogenetic characteristics, impacting by the gene mutation, gene copy number alteration, neoantigens, as well as the infiltration of immunocytes. Several teams established the molecular classifications among bladder cancer. Mo et al.[38]generated a tumor 18-gene signature in MIBC patients, which could reflect the urothelial differentiation and predict the clinical outcomes, basal and differentiated groups was named to the two group with high or low risk score, respectively. Damrauer *et al.*[39] developed BASE47, a transcriptomic classifier using 47 genes, to classify the MIBC tumor into luminal-like or basal-like subtype. Robertson et al.[40] performed a Bayesian NMF with consensus hierarchical clustering in 408 MIBC tumors from TCGA and found five expression subtypes, including three luminal subtypes (named Luminal-papillary, Luminal-Infiltrated and Luminal), Basal/Squamous subtype, and Neuronal subtype. However, most of the molecular classifiers only focused

on the clinical outcomes, but not the tumor immune microenvironment. Therefore, our goal is to provide a comprehensive insight to the immune response of bladder cancer patients with diverse inner molecular features, and help to find the suitable patients undergo the precise immunotherapy.

NMF algorithm is an unsupervised, parts-based learning paradigm, which could decompose a nonnegative matrix V into two nonnegative matrices, W and H, via a multiplicative updates algorithm[41]. Similarly to principal components analysis (PCA) or independent component analysis (ICA), the objective of NMF is to explain the observed data using a limited number of basic components, which could reflect the original data as accurately as possible[42]. NMF was applied to reveal the biomarkers, classify the tumor subtypes and predict the prognosis of tumors recent days[43-45]. As for the enrolled 4,003 bladder cancer patients. We investigated a robust classification of three immunophenotypes based on the NMF algorithm. Firstly, we identified the immune activated subgroup, immune exhausted subgroup and non-immune class in the 408 bladder cancer patients from TCGA-BLCA cohort. The 150 exemplar genes from immune module represented the immune feature in bladder cancer patients and further divide the whole cohort to immune and non-immune classes. The other 150 DEGs among the immune and non-immune classes was extracted as the input profile for the validation of the classification in external 19 cohorts. As to the distinguish of immune activated and immune exhausted subgroup, a stromal activation signature was conducted by NTP algorithm. The features of these three immunophenotypes was illuminated by several verified signatures of immunocytes or immune signaling pathways. Patients in the immune classes shown the highly enriched signatures of T cell, B cell, IFN and CYT[46-48], while the exhausted subgroup also shown an increased signature of TITR, WNT/TGF-β, TGF-β1 activated, and C-ECM signatures[49-51], but not the immune activated subgroup. Totally,

362 based on our results, we revealed that there are only about 11% to 30.9% bladder cancer
363 patients belong to the immune activated subgroup, which might response to the
364 immunotherapy.

365 Clinical outcome is an important factor we focused about the newly defined
366 immunophenotypes. With the clinical information of TCGA-BLCA, GSE32894, E-MTAB-
367 1803 and GSE13507 cohorts, we generated the results that patients belong to the immune
368 activated subgroup contain the best overall survival, while the immune exhausted
369 subgroup shown the worst clinical outcome of a shorten overall survival time. Immune
370 exhausted, mostly focused on the exhausted of T cell, reflected by the altered
371 inflammatory and tissue microenvironments, lymphocyte, as well as the inhibitory signals
372 from cytokines[52]. These alternations in the TIME could lead to the escape of the immune
373 recognition by blocking of the immune checkpoints, and related with the unfavorable
374 overall survival for patients[53]. We predicted the potential response to immunotherapy of
375 the bladder cancer patients by compared the mRNA expression profile with melanoma
376 samples receiving anti-CTLA-4 or anti-PD-1 checkpoint therapy. As expected, patients in
377 the immune activated subgroup could benefit from the treatment of an-PD-1 therapy, but
378 not the non-immune activated subgroup, which combined the immune exhausted and non-
379 immune classes.

380 To further understanding the molecular diverse among there three immunophenotypes,
381 we compared the CNA, TMB, and gene mutations. Recent studies report the association
382 of CNA with the increased immune infiltration and the outcome of immune checkpoint
383 blockade therapy[54,55]. Patients in the immune class shown a lower CNA burden in gene
384 deletion among arm- and focal-level. The association was double checked by that the
385 deletion copy number of PD-1, PD-L1 and CTLA4 is positively with the decrease infiltration
386 level of immunocytes. Tripathi et al.[56] found that antigen presentation through MHC class

I pathway is suppressed in tumors with high chromosomal instability, also known as the high CNA, which acts as a pivotal role in the immune evasion. In addition, Lu et al.[57] revealed that patients treated with immune-checkpoint-blockade therapy could get a durable clinical benefit and better survival, if the contains the lower burden of CNA. Gene mutation is another key component we focused among the three immunophenotypes. We extracted the specific mutant genes for each subgroup. The proportion of mutant TP53, TTN, PIC3CA and RB1 is higher in immune class than non-immune class. Nusrat et al.[58] reported that colorectal cancer patients with the mutant PIK3CA have a higher median density of CD3+ and CD8+ cells, as well as a high rate of clinical benefit form immunotherapy (50% vs. 8.6%). What's more, we observed the high rate of ERBB2 mutation in immune activated subgroup. ERBB2 amplification or overexpression was a biomarker of anti-ERBB2 target therapy in breast cancer, the activated ERBB2 oncogene regulates recruitment and activation of tumor infiltrating immune cells and trastuzumab activity by inducing CCL2 and PD-1 ligands[59]. The V659E mutation of ERBB2 gene was also reported associated with the altering sensitivity of afatinib and lapatinib treatment in in vitro[60,61]. The mutation proportion of EP300 is highest in immune exhausted subgroup. Recent research concerned the importance of CBP/EP300 in regulatory T cells (Treg), because conditional deletion of either EP300 or CBP in mouse Tregs led to impaired Treg suppressive function[62]. Intratumoral Tregs dampen effector T cell responses to tumor antigens, engendering an immunosuppressive microenvironment, and linked with a poor prognosis in tumors[63].

We defined and validated a novel classifier among the 4003 bladder cancer patients, to separate the bladder cancer patients to immune activated, immune suppressed and non-immune subgroups. Patients in the immune activated subgroup could benefit more from the single treatment of anti-PD-1 immunotherapy; As to the immune exhausted subgroup,

ICB therapy plus TGF-β inhibitor or EP300 inhibitor might be more effectiveness. In summary, our novel classifier provide illumination for the enhancing immunotherapy of bladder cancer patients.

Data availability statement

All data used in this work can be acquired from the GDC portal (https://portal.gdc.cancer.gov/), Gene-Expression Omni-bus (GEO; https://www.ncbi.nlm.nih.gov/geo/), and ArrayExpress (https://www.ebi.ac.uk/arrayexpress/).

Acknowledgements

This work was supported by the National Natural Science Foundation of China [grant number: 81802827, 81630019, 31701162]; Scientific Research Foundation of the Institute for Translational Medicine of Anhui Province [grant number: 2017ZHYX02]; The Natural Science Foundation of Guangdong Province, China [grant number: 2017A030313800]; The Key Project of Provincial Natural Science Research Project of Anhui Colleges [grant number: KJ2019A0278]; Supporting Project for Distinguished Young Scholar of Anhui Colleges [grant number: gxyqZD2019018]; 2017 Anhui Province special program for guiding local science and technology development by the central government [grant number: 2017070802D148].

Conflict of interests

The authors have declared no conflicts of interest.

Ethics approval

The patient data in this work acquired from the publicly available datasets whose informed consent of patients were complete. For the AHMU-PC cohort, the research contents and research programs were reviewed and approved by the Ethics Committee of the First Affiliated Hospital of Anhui Medical University (PJ-2019-09-11), patient consent for the retrospective cohorts was waived.

Authors' contributions

Conception and Design: Jialin Meng, Xiaofan Lu, Fangrong Yan and Chaozhao Liang. Collection and Assembly of Data: Yujie Zhou, Xiaofan Lu, Meng Zhang, Yinan Du, Jun Zhou. Data Analysis and Interpretation: Jialin Meng, Yujie Zhou, Xiaofan Lu, Zongyao Hao. Manuscript Writing: Jialin Meng, Xiaofan Lu, Yujie Zhou, Meng Zhang. Final Approval of Manuscript: All the authors.

REFERENCES:

1 Sanchez, A. *et al.* Incidence, Clinicopathological Risk Factors, Management and Outcomes of Nonmuscle Invasive Recurrence after Complete Response to Trimodality Therapy for Muscle Invasive Bladder Cancer. *J Urol* **199**, 407-415, doi:10.1016/j.juro.2017.08.106 (2018).

2 Bray, F. *et al.* Global cancer statistics 2018: GLOBOCAN estimates of incidence and mortality worldwide for 36 cancers in 185 countries. *CA Cancer J Clin* **68**, 394-424, doi:10.3322/caac.21492 (2018).

3 Siegel, R. L., Miller, K. D. & Jemal, A. Cancer statistics, 2020. *CA Cancer J Clin* **70**, 7-30, doi:10.3322/caac.21590 (2020).

4 Kamat, A. M. *et al.* Bladder cancer. *Lancet* **388**, 2796-2810, doi:10.1016/S0140-6736(16)30512-8 (2016).

5 Gandhi, N. M., Morales, A. & Lamm, D. L. Bacillus Calmette-Guerin immunotherapy for genitourinary cancer. *BJU Int* **112**, 288-297, doi:10.1111/j.1464-410X.2012.11754.x (2013).

6 Bellmunt, J. *et al.* Bladder cancer: ESMO Practice Guidelines for diagnosis, treatment and follow-up. *Ann Oncol* **25 Suppl 3**, iii40-48, doi:10.1093/annonc/mdu223 (2014).

7 Chamie, K. *et al.* Recurrence of high-risk bladder cancer: a population-based analysis. *Cancer* **119**, 3219-3227, doi:10.1002/cncr.28147 (2013).

8 Pectasides, D., Pectasides, M. & Nikolaou, M. Adjuvant and neoadjuvant chemotherapy in muscle invasive bladder cancer: literature review. *Eur Urol* **48**, 60-67; discussion 67-68, doi:10.1016/j.eururo.2005.03.025 (2005).

9 Kalinski, P. *Tumor Immune Microenvironment in Cancer Progression and Cancer Therapy*. Vol. 1036 (Springer International Publishing, 2017).

10 Akaza, H. BCG treatment of existing Ta, T1 tumours or carcinoma in situ of the bladder. *Eur Urol* **27 Suppl 1**, 9-12, doi:10.1159/000475202 (1995).
11 Balar, A. V. *et al.* Atezolizumab as first-line treatment in cisplatin-ineligible patients with locally advanced and metastatic urothelial carcinoma: a single-arm, multicentre, phase 2 trial. *Lancet* **389**, 67-76, doi:10.1016/S0140-6736(16)32455-2 (2017).
12 Rosenberg, J. E. *et al.* Atezolizumab in patients with locally advanced and metastatic urothelial carcinoma who have progressed following treatment with platinum-based chemotherapy: a single-arm, multicentre, phase 2 trial. *Lancet* **387**, 1909-1920, doi:10.1016/S0140-6736(16)00561-4 (2016).
13 Sharma, P. *et al.* Nivolumab monotherapy in recurrent metastatic urothelial carcinoma (CheckMate 032): a multicentre, open-label, two-stage, multi-arm, phase 1/2 trial. *Lancet Oncol* **17**, 1590-1598, doi:10.1016/S1470-2045(16)30496-X (2016).
14 Sharma, P. *et al.* Nivolumab in metastatic urothelial carcinoma after platinum therapy (CheckMate 275): a multicentre, single-arm, phase 2 trial. *Lancet Oncol* **18**, 312-322, doi:10.1016/S1470-2045(17)30065-7 (2017).
15 Powles, T. *et al.* Efficacy and Safety of Durvalumab in Locally Advanced or Metastatic Urothelial Carcinoma: Updated Results From a Phase 1/2 Open-label Study. *JAMA Oncol* **3**, e172411, doi:10.1001/jamaoncol.2017.2411 (2017).
16 Patel, M. R. *et al.* Avelumab in metastatic urothelial carcinoma after platinum failure (JAVELIN Solid Tumor): pooled results from two expansion cohorts of an open-label, phase 1 trial. *Lancet Oncol* **19**, 51-64, doi:10.1016/S1470-2045(17)30900-2 (2018).
17 Lee, D. D. & Seung, H. S. Learning the parts of objects by non-negative matrix factorization. *Nature* **401**, 788-791, doi:10.1038/44565 (1999).
18 Yoshihara, K. *et al.* Inferring tumour purity and stromal and immune cell admixture from expression data. *Nat Commun* **4**, 2612, doi:10.1038/ncomms3612 (2013).
19 Sia, D. *et al.* Identification of an Immune-specific Class of Hepatocellular Carcinoma, Based on Molecular Features. *Gastroenterology* **153**, 812-826, doi:10.1053/j.gastro.2017.06.007 (2017).
20 Moffitt, R. A. *et al.* Virtual microdissection identifies distinct tumor- and stroma-specific subtypes of pancreatic ductal adenocarcinoma. *Nat Genet* **47**, 1168-1178, doi:10.1038/ng.3398 (2015).
21 Valkenburg, K. C., de Groot, A. E. & Pienta, K. J. Targeting the tumour stroma to improve cancer therapy. *Nat Rev Clin Oncol* **15**, 366-381, doi:10.1038/s41571-018-0007-1 (2018).
22 Hanahan, D. & Coussens, L. M. Accessories to the crime: functions of cells recruited to the tumor microenvironment. *Cancer Cell* **21**, 309-322, doi:10.1016/j.ccr.2012.02.022 (2012).
23 Sivanathan, K. N., Gronthos, S., Rojas-Canales, D., Thierry, B. & Coates, P. T. Interferon-gamma modification of mesenchymal stem cells: implications of autologous and allogeneic mesenchymal stem cell therapy in allotransplantation. *Stem Cell Rev Rep* **10**, 351-375, doi:10.1007/s12015-014-9495-2 (2014).
24 van Megen, K. M. *et al.* Activated Mesenchymal Stromal Cells Process and Present Antigens Regulating Adaptive Immunity. *Front Immunol* **10**, 694, doi:10.3389/fimmu.2019.00694 (2019).
25 Soboslay, P. T. *et al.* Regulatory effects of Th1-type (IFN-gamma, IL-12) and Th2-type cytokines (IL-10, IL-13) on parasite-specific cellular responsiveness in

Onchocerca volvulus-infected humans and exposed endemic controls. *Immunology* **97**, 219-225, doi:10.1046/j.1365-2567.1999.00018.x (1999).

26 Aggarwal, S. & Pittenger, M. F. Human mesenchymal stem cells modulate allogeneic immune cell responses. *Blood* **105**, 1815-1822, doi:10.1182/blood-2004-04-1559 (2005).

27 Selleri, S. *et al.* Cord-blood-derived mesenchymal stromal cells downmodulate CD4+ T-cell activation by inducing IL-10-producing Th1 cells. *Stem Cells Dev* **22**, 1063-1075, doi:10.1089/scd.2012.0315 (2013).

28 Batlle, E. & Massague, J. Transforming Growth Factor-beta Signaling in Immunity and Cancer. *Immunity* **50**, 924-940, doi:10.1016/j.immuni.2019.03.024 (2019).

29 Furukawa, A., Wisel, S. A. & Tang, Q. Impact of Immune-Modulatory Drugs on Regulatory T Cell. *Transplantation* **100**, 2288-2300, doi:10.1097/TP.0000000000001379 (2016).

30 Groth, C. *et al.* Immunosuppression mediated by myeloid-derived suppressor cells (MDSCs) during tumour progression. *Br J Cancer* **120**, 16-25, doi:10.1038/s41416-018-0333-1 (2019).

31 Berraondo, P. *et al.* Cytokines in clinical cancer immunotherapy. *Br J Cancer* **120**, 6-15, doi:10.1038/s41416-018-0328-y (2019).

32 Dong, Y. *et al.* CD4(+) T cell exhaustion revealed by high PD-1 and LAG-3 expression and the loss of helper T cell function in chronic hepatitis B. *BMC Immunol* **20**, 27, doi:10.1186/s12865-019-0309-9 (2019).

33 Liu, J. F. *et al.* Blockade of TIM3 relieves immunosuppression through reducing regulatory T cells in head and neck cancer. *J Exp Clin Cancer Res* **37**, 44, doi:10.1186/s13046-018-0713-7 (2018).

34 Saltz, J. *et al.* Spatial Organization and Molecular Correlation of Tumor-Infiltrating Lymphocytes Using Deep Learning on Pathology Images. *Cell Rep* **23**, 181-193 e187, doi:10.1016/j.celrep.2018.03.086 (2018).

35 Thorsson, V. *et al.* The Immune Landscape of Cancer. *Immunity* **48**, 812-830 e814, doi:10.1016/j.immuni.2018.03.023 (2018).

36 Kamoun, A. *et al.* A Consensus Molecular Classification of Muscle-invasive Bladder Cancer. *Eur Urol* **77**, 420-433, doi:10.1016/j.eururo.2019.09.006 (2020).

37 Hautmann, R. E., Gschwend, J. E., de Petriconi, R. C., Kron, M. & Volkmer, B. G. Cystectomy for transitional cell carcinoma of the bladder: results of a surgery only series in the neobladder era. *J Urol* **176**, 486-492; discussion 491-482, doi:10.1016/j.juro.2006.03.038 (2006).

38 Mo, Q. *et al.* Prognostic Power of a Tumor Differentiation Gene Signature for Bladder Urothelial Carcinomas. *J Natl Cancer Inst* **110**, 448-459, doi:10.1093/jnci/djx243 (2018).

39 Damrauer, J. S. *et al.* Intrinsic subtypes of high-grade bladder cancer reflect the hallmarks of breast cancer biology. *Proc Natl Acad Sci U S A* **111**, 3110-3115, doi:10.1073/pnas.1318376111 (2014).

40 Robertson, A. G. *et al.* Comprehensive Molecular Characterization of Muscle-Invasive Bladder Cancer. *Cell* **171**, 540-556 e525, doi:10.1016/j.cell.2017.09.007 (2017).

41 Devarajan, K. Nonnegative matrix factorization: an analytical and interpretive tool in computational biology. *PLoS Comput Biol* **4**, e1000029, doi:10.1371/journal.pcbi.1000029 (2008).

42 Gaujoux, R. & Seoighe, C. A flexible R package for nonnegative matrix factorization. *BMC Bioinformatics* **11**, 367, doi:10.1186/1471-2105-11-367 (2010).

43 Zeng, Z. *et al.* Cancer classification and pathway discovery using non-negative matrix factorization. *J Biomed Inform* **96**, 103247, doi:10.1016/j.jbi.2019.103247 (2019).

44 Esposito, F., Boccarelli, A. & Del Buono, N. An NMF-Based Methodology for Selecting Biomarkers in the Landscape of Genes of Heterogeneous Cancer-Associated Fibroblast Populations. *Bioinform Biol Insights* **14**, 1177932220906827, doi:10.1177/1177932220906827 (2020).

45 Meng, J. *et al.* Immune Response Drives Outcomes in Prostate Cancer: Implications for Immunotherapy. *bioRxiv*, 2020.2005.2026.117218, doi:10.1101/2020.05.26.117218 (2020).

46 Iglesia, M. D. *et al.* Prognostic B-cell signatures using mRNA-seq in patients with subtype-specific breast and ovarian cancer. *Clin Cancer Res* **20**, 3818-3829, doi:10.1158/1078-0432.CCR-13-3368 (2014).

47 Bindea, G. *et al.* Spatiotemporal dynamics of intratumoral immune cells reveal the immune landscape in human cancer. *Immunity* **39**, 782-795, doi:10.1016/j.immuni.2013.10.003 (2013).

48 Chow, L. Q. M. *et al.* Biomarkers and response to pembrolizumab (pembro) in recurrent/metastatic head and neck squamous cell carcinoma (R/M HNSCC). *Journal of Clinical Oncology* **34**, 6010-6010, doi:10.1200/JCO.2016.34.15_suppl.6010 (2016).

49 Magnuson, A. M. *et al.* Identification and validation of a tumor-infiltrating Treg transcriptional signature conserved across species and tumor types. *Proc Natl Acad Sci U S A* **115**, E10672-E10681, doi:10.1073/pnas.1810580115 (2018).

50 Lachenmayer, A. *et al.* Wnt-pathway activation in two molecular classes of hepatocellular carcinoma and experimental modulation by sorafenib. *Clin Cancer Res* **18**, 4997-5007, doi:10.1158/1078-0432.CCR-11-2322 (2012).

51 Chakravarthy, A., Khan, L., Bensler, N. P., Bose, P. & De Carvalho, D. D. TGF-beta-associated extracellular matrix genes link cancer-associated fibroblasts to immune evasion and immunotherapy failure. *Nat Commun* **9**, 4692, doi:10.1038/s41467-018-06654-8 (2018).

52 Wherry, E. J. & Kurachi, M. Molecular and cellular insights into T cell exhaustion. *Nat Rev Immunol* **15**, 486-499, doi:10.1038/nri3862 (2015).

53 Sharma, P., Hu-Lieskovan, S., Wargo, J. A. & Ribas, A. Primary, Adaptive, and Acquired Resistance to Cancer Immunotherapy. *Cell* **168**, 707-723, doi:10.1016/j.cell.2017.01.017 (2017).

54 Chan, T. A., Wolchok, J. D. & Snyder, A. Genetic Basis for Clinical Response to CTLA-4 Blockade in Melanoma. *N Engl J Med* **373**, 1984, doi:10.1056/NEJMc1508163 (2015).

55 Davoli, T., Uno, H., Wooten, E. C. & Elledge, S. J. Tumor aneuploidy correlates with markers of immune evasion and with reduced response to immunotherapy. *Science* **355**, doi:10.1126/science.aaf8399 (2017).

56 Tripathi, R., Modur, V., Senovilla, L., Kroemer, G. & Komurov, K. Suppression of tumor antigen presentation during aneuploid tumor evolution contributes to immune evasion. *Oncoimmunology* **8**, 1657374, doi:10.1080/2162402X.2019.1657374 (2019).

57 Lu, Z. *et al.* Tumor copy-number alterations predict response to immune-checkpoint-blockade in gastrointestinal cancer. *J Immunother Cancer* **8**, doi:10.1136/jitc-2019-000374 (2020).

58 Nusrat, M. *et al.* Association of PIK3CA mutations (mut) with immune engagement and clinical benefit from immunotherapy in microsatellite stable

(MSS) colorectal cancer (CRC) patients (pts). *Journal of Clinical Oncology* **37**, 3604-3604, doi:10.1200/JCO.2019.37.15_suppl.3604 (2019).

59 Triulzi, T. *et al.* HER2 signaling regulates the tumor immune microenvironment and trastuzumab efficacy. *Oncoimmunology* **8**, e1512942, doi:10.1080/2162402X.2018.1512942 (2019).

60 Serra, V. *et al.* Clinical response to a lapatinib-based therapy for a Li-Fraumeni syndrome patient with a novel HER2V659E mutation. *Cancer Discov* **3**, 1238-1244, doi:10.1158/2159-8290.CD-13-0132 (2013).

61 Yamamoto, H. *et al.* Therapeutic Potential of Afatinib for Cancers with ERBB2 (HER2) Transmembrane Domain Mutations G660D and V659E. *Oncologist* **23**, 150-154, doi:10.1634/theoncologist.2017-0345 (2018).

62 Liu, Y. *et al.* Two histone/protein acetyltransferases, CBP and p300, are indispensable for Foxp3+ T-regulatory cell development and function. *Mol Cell Biol* **34**, 3993-4007, doi:10.1128/MCB.00919-14 (2014).

63 Curiel, T. J. *et al.* Specific recruitment of regulatory T cells in ovarian carcinoma fosters immune privilege and predicts reduced survival. *Nat Med* **10**, 942-949, doi:10.1038/nm1093 (2004).

Figure Legends

Figure 1. The flow chart demonstrates the summary of performed analysis in this study. A total of 4,003 bladder cancer patients from 20 cohorts with the mRNA expression profile were enrolled for the analysis, with non-negative matrix factorization algorithm and nearest template prediction, three immunophenotypes were generated in TCGA-BLCA cohort, and validated in 19 external cohorts. The molecular characteristic, prognosis and response to immunotherapy are difference in the three subtypes. NMF, non-negative matrix factorization; TCGA-BLCA, The Cancer Genome Atlas-prostate adenocarcinoma bladder cancer; TIL, tumor-infiltrating lymphocytes; CNA, copy number alteration; TMB, tumor mutation burden.

Figure 2. Recognition the immune classes by non-negative matrix factorization (NMF) algorithm

(A) Nine modules generated from the NMF algorithm, patients with high immune enrichment score gathered in the immune module; (B) Heatmap showing the top 150 exemplar genes expression among immune enriched and non-immune enriched clusters, divided by consensus clustering; (C) the multidimensional scaling (MDS) random forest further modified the clusters to immune and non-immune classes; (D) The distribution of patients in different NMF modules, immune module weight, exemplar gene clustering, final immune classes and immune enrichment score.

Figure 3. The diverse immune characteristics of non-immune class, immune activated subgroup, and immune exhausted subgroup.

Immune class (253/408, 62.0%) and non-immune class (155/408, 38.0%) were distinguished by the consensus clustering and multidimensional scaling random forest based on the 150 exemplar genes obtained from the non-negative matrix factorization algorithm generated immune module; The immune activated subgroup (45/408, 11.0%) and immune exhausted subgroup (110/408, 27.0%) further divided by the stromal activation signature with nearest template prediction analysis. The high and low gene set enrichment scores are displayed with red and green, respectively. The details of these immune associated signatures listed in Table S2. TCGA-BLCA, The Cancer Genome Atlas-bladder cancer; CYT, cytolytic activity score; TITR, tumor-infiltrating Tregs; MDSC, myeloid-derived suppressor cell; TLS, tertiary lymphoid structure; C-ECM, cancer-associated extracellular matrix.

Figure 4. The heterogeneity of genetic phenotypes of non-immune class, immune activated subgroup, and immune exhausted subgroup.

(A) Difference of tumor-infiltrating lymphocytes abundance; (B) Difference of PD-L1 mRNA expression level; (C) Difference of gene copy number alterations, including amplification and deletion, among arm-level and focal level; (D) Difference of tumor mutation burden; (E) Difference of neoantigens; (F) Different distribution of mutant genes in three immunophenotypes.

Figure 5. The specific mutant genes of non-immune class, immune activated subgroup, and immune exhausted subgroup.

(A) TP53, TTN, PIK3CA and RB1 are the specific mutant genes in immune class compared with non-immune class; (B) ERBB2, KMT2A, PKHD1 and MDN1 are the specific mutant genes in immune activated subgroup; (C) EP300, HMCN1, AKAP9 and MACF1 are the specific mutant genes in immune exhausted subgroup. IM, immune class;

695 Non-IM, non-immune class; IM-Act, immune activated subgroup; IM-Exh, immune
696 exhausted subgroup.

697 **Figure 6. Reappearing the diverse immune characteristics of three**
698 **immunophenotypes in GSE32894 cohort.**

699 CYT, cytolytic activity score; TITR, tumor-infiltrating Tregs; MDSC, myeloid-derived
700 suppressor cell; TLS, tertiary lymphoid structure; C-ECM, cancer-associated extracellular
701 matrix.

702 **Figure 7. Immunophenotypes indicate separated overall survival outcome and**
703 **response to immunotherapy for bladder cancer patients**

704 (A) Different overall survival outcome in three immunophenotypes among patients high
705 than 70 years old in TCGA-BLCA cohort, GSE32894 cohort, E-MTAB-1803 cohort, and
706 GSE13507 cohort; (B) Subclass mapping analysis manifested that patients with immune
707 activated subtype were more likely to respond to anti–PD-1 treatment.

708 **Figure 8. Correlate the three immunophenotypes with proposed molecular subtypes.**

709 (A) Association with Thorsson et al. generated pan-cancer six immune molecular features;
710 (B) Association with Kamoun et al. identified the consensus set of six molecular classes.

711 **Figure S1. GSEA results showing the activated signaling pathways in the immune**
712 **class.** NES, normalized enrichment score; FDR, false discovery rate; FDR less than
713 0.05 indicates statistical significance.

Figure S2. Stromal representative signatures and markers in immune activated and exhausted subgroups. ****, $P < 0.0001$; ***, $P < 0.001$; **, $P < 0.01$; *, $P < 0.05$; ns, no significance.

Figure S3. The association between copy number variation of immune checkpoints and immunocyte infiltration. ***, $P < 0.001$; **, $P < 0.01$; *, $P < 0.05$.

Figure S4. Successful validation of the immunophenotypes among the E-MTAB-4321 cohort. CYT, cytolytic activity score; TITR, tumor-infiltrating Tregs; MDSC, myeloid-derived suppressor cell; TLS, tertiary lymphoid structure; C-ECM, cancer-associated extracellular matrix.

Figure S5. Successful validation of the immunophenotypes among the IMvigor210 cohort. CYT, cytolytic activity score; TITR, tumor-infiltrating Tregs; MDSC, myeloid-derived suppressor cell; TLS, tertiary lymphoid structure; C-ECM, cancer-associated extracellular matrix.

Figure S6. Successful validation of the immunophenotypes among the GSE83586 cohort. CYT, cytolytic activity score; TITR, tumor-infiltrating Tregs; MDSC, myeloid-derived suppressor cell; TLS, tertiary lymphoid structure; C-ECM, cancer-associated extracellular matrix.

Figure S7. Successful validation of the immunophenotypes among the GSE87304 cohort. CYT, cytolytic activity score; TITR, tumor-infiltrating Tregs; MDSC, myeloid-derived suppressor cell; TLS, tertiary lymphoid structure; C-ECM, cancer-associated extracellular matrix.

Figure S8. Successful validation of the immunophenotypes among the GSE128702 cohort. CYT, cytolytic activity score; TITR, tumor-infiltrating Tregs; MDSC, myeloid-

737 derived suppressor cell; TLS, tertiary lymphoid structure; C-ECM, cancer-associated
738 extracellular matrix.

739 **Figure S9. Successful validation of the immunophenotypes among the GSE13507**
740 **cohort.** CYT, cytolytic activity score; TITR, tumor-infiltrating Tregs; MDSC, myeloid-
741 derived suppressor cell; TLS, tertiary lymphoid structure; C-ECM, cancer-associated
742 extracellular matrix.

743 **Figure S10. Successful validation of the immunophenotypes among the GSE120736**
744 **cohort.** CYT, cytolytic activity score; TITR, tumor-infiltrating Tregs; MDSC, myeloid-
745 derived suppressor cell; TLS, tertiary lymphoid structure; C-ECM, cancer-associated
746 extracellular matrix.

747 **Figure S11. Successful validation of the immunophenotypes among the GSE39016**
748 **cohort.** CYT, cytolytic activity score; TITR, tumor-infiltrating Tregs; MDSC, myeloid-
749 derived suppressor cell; TLS, tertiary lymphoid structure; C-ECM, cancer-associated
750 extracellular matrix.

751 **Figure S12. Successful validation of the immunophenotypes among the GSE128701**
752 **cohort.** CYT, cytolytic activity score; TITR, tumor-infiltrating Tregs; MDSC, myeloid-
753 derived suppressor cell; TLS, tertiary lymphoid structure; C-ECM, cancer-associated
754 extracellular matrix.

755 **Figure S13. Successful validation of the immunophenotypes among the GSE124035**
756 **cohort.** CYT, cytolytic activity score; TITR, tumor-infiltrating Tregs; MDSC, myeloid-
757 derived suppressor cell; TLS, tertiary lymphoid structure; C-ECM, cancer-associated
758 extracellular matrix.

Figure S14. Successful validation of the immunophenotypes among the GSE86411 cohort. CYT, cytolytic activity score; TITR, tumor-infiltrating Tregs; MDSC, myeloid-derived suppressor cell; TLS, tertiary lymphoid structure; C-ECM, cancer-associated extracellular matrix.

Figure S15. Successful validation of the immunophenotypes among the GSE48276 cohort. CYT, cytolytic activity score; TITR, tumor-infiltrating Tregs; MDSC, myeloid-derived suppressor cell; TLS, tertiary lymphoid structure; C-ECM, cancer-associated extracellular matrix.

Figure S16. Successful validation of the immunophenotypes among the GSE31684 cohort. CYT, cytolytic activity score; TITR, tumor-infiltrating Tregs; MDSC, myeloid-derived suppressor cell; TLS, tertiary lymphoid structure; C-ECM, cancer-associated extracellular matrix.

Figure S17. Successful validation of the immunophenotypes among the GSE134292 cohort. CYT, cytolytic activity score; TITR, tumor-infiltrating Tregs; MDSC, myeloid-derived suppressor cell; TLS, tertiary lymphoid structure; C-ECM, cancer-associated extracellular matrix.

Figure S18. Successful validation of the immunophenotypes among the GSE93257 cohort. CYT, cytolytic activity score; TITR, tumor-infiltrating Tregs; MDSC, myeloid-derived suppressor cell; TLS, tertiary lymphoid structure; C-ECM, cancer-associated extracellular matrix.

Figure S19. Successful validation of the immunophenotypes among the E-MTAB-1803 cohort. CYT, cytolytic activity score; TITR, tumor-infiltrating Tregs; MDSC, myeloid-

781 derived suppressor cell; TLS, tertiary lymphoid structure; C-ECM, cancer-associated
782 extracellular matrix.

783 **Figure S20. Successful validation of the immunophenotypes among the GSE69795**
784 **cohort.** CYT, cytolytic activity score; TITR, tumor-infiltrating Tregs; MDSC, myeloid-
785 derived suppressor cell; TLS, tertiary lymphoid structure; C-ECM, cancer-associated
786 extracellular matrix.

787 **Figure S21. Successful validation of the immunophenotypes among the GSE129871**
788 **cohort.** CYT, cytolytic activity score; TITR, tumor-infiltrating Tregs; MDSC, myeloid-
789 derived suppressor cell; TLS, tertiary lymphoid structure; C-ECM, cancer-associated
790 extracellular matrix.

791

792

793

794

795

796

797

798

799

800

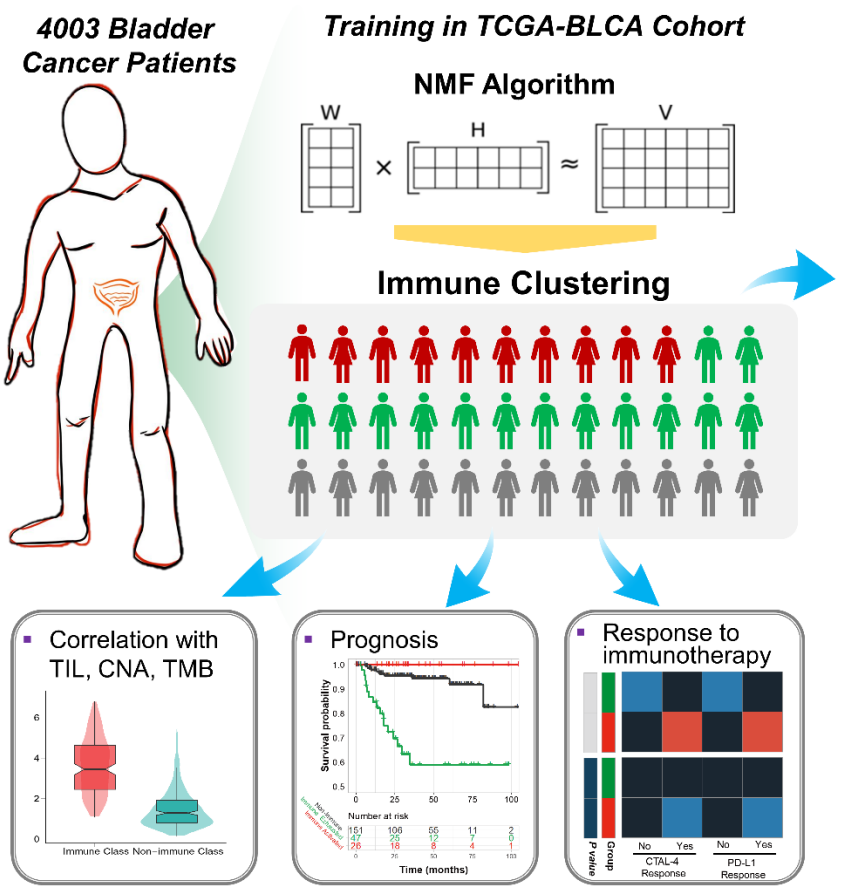

Validation in 19 External Cohorts

Dataset	N
E-MTAB-4321	476
IMvigor210	348
GSE32894	308
GSE83586	307
GSE87304	305
GSE128702	256
GSE13507	164
GSE129871	158
GSE120736	145
GSE39016	141
GSE128701	136
GSE124035	133
GSE86411	132
GSE48276	116
GSE31684	93
GSE134292	80
GSE93527	79
E-MTAB-1803	70
GSE69795	61

Figure 1

801

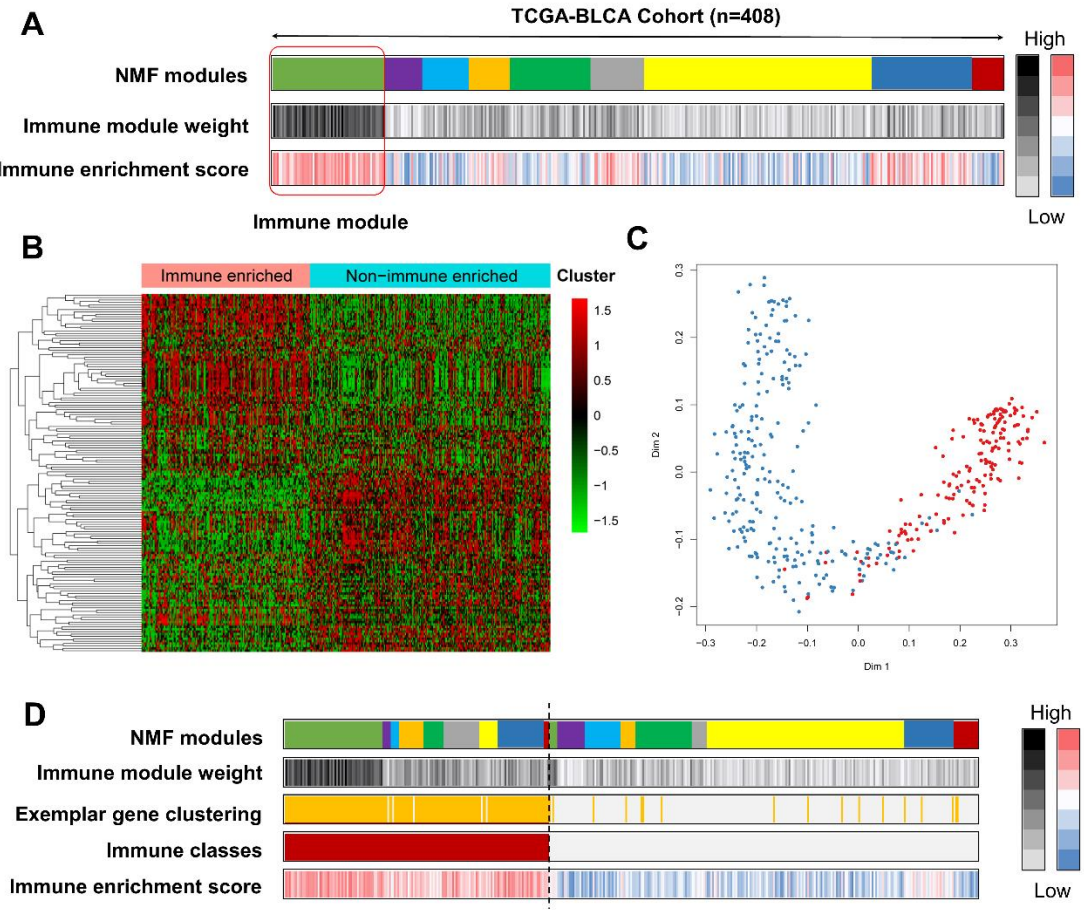

Figure 2

802

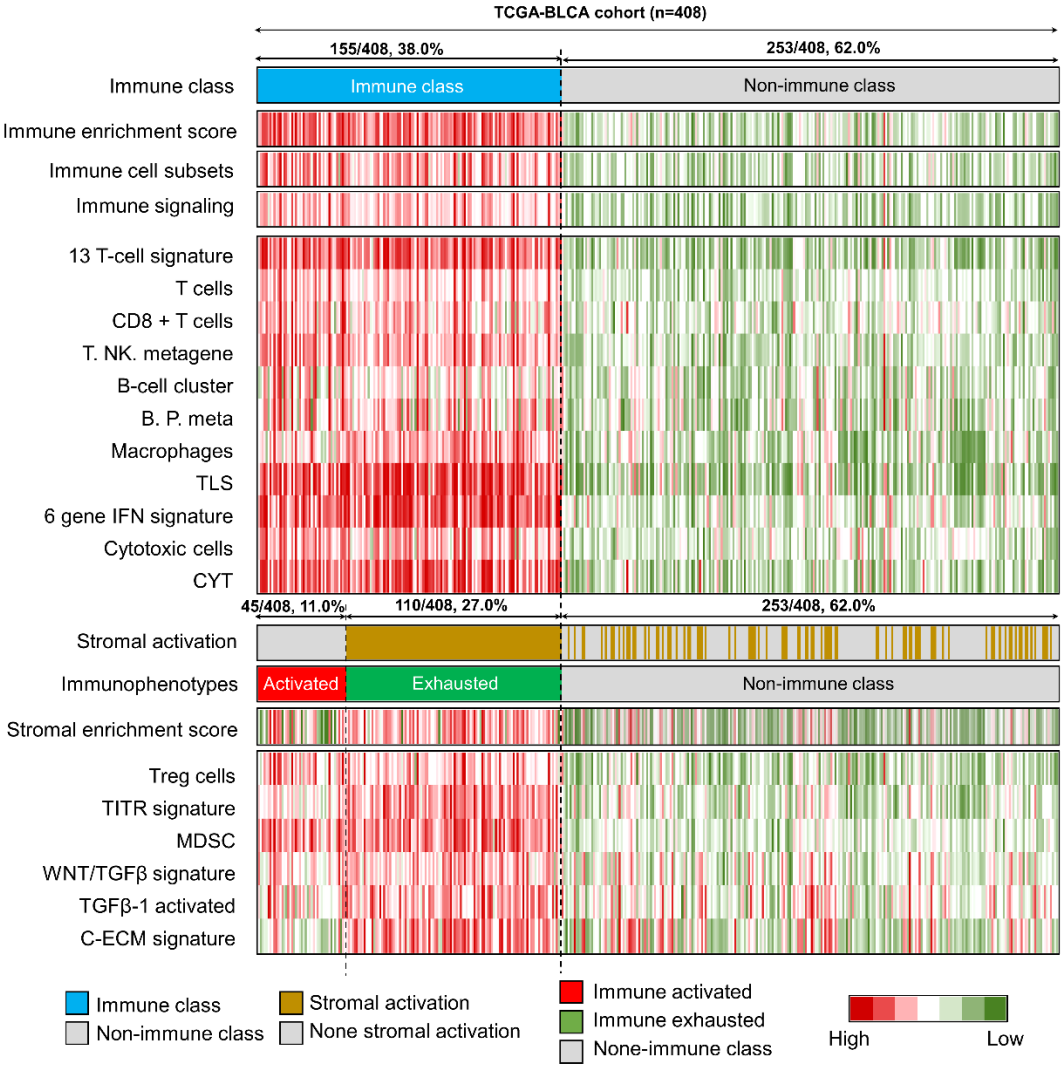

Figure 3

803

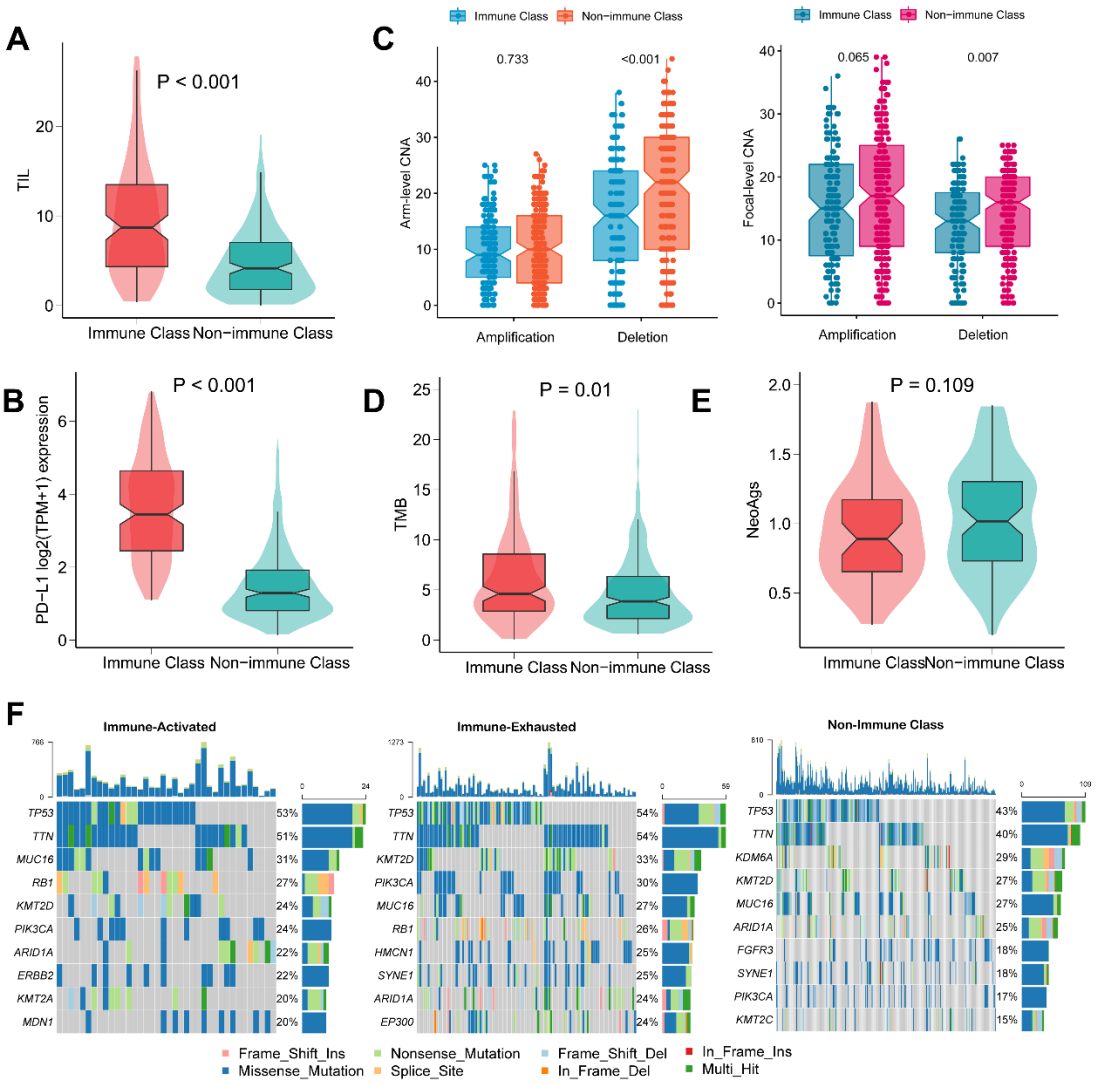

Figure 4

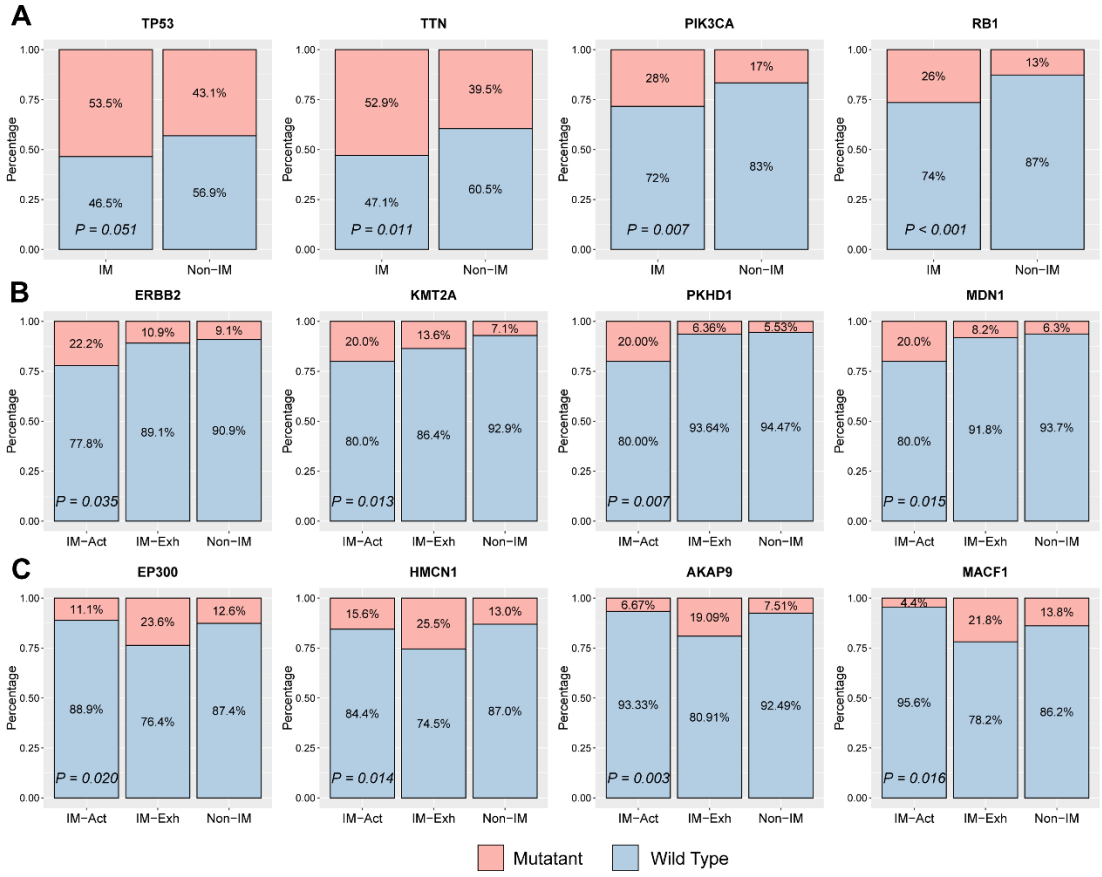

Figure 5

805

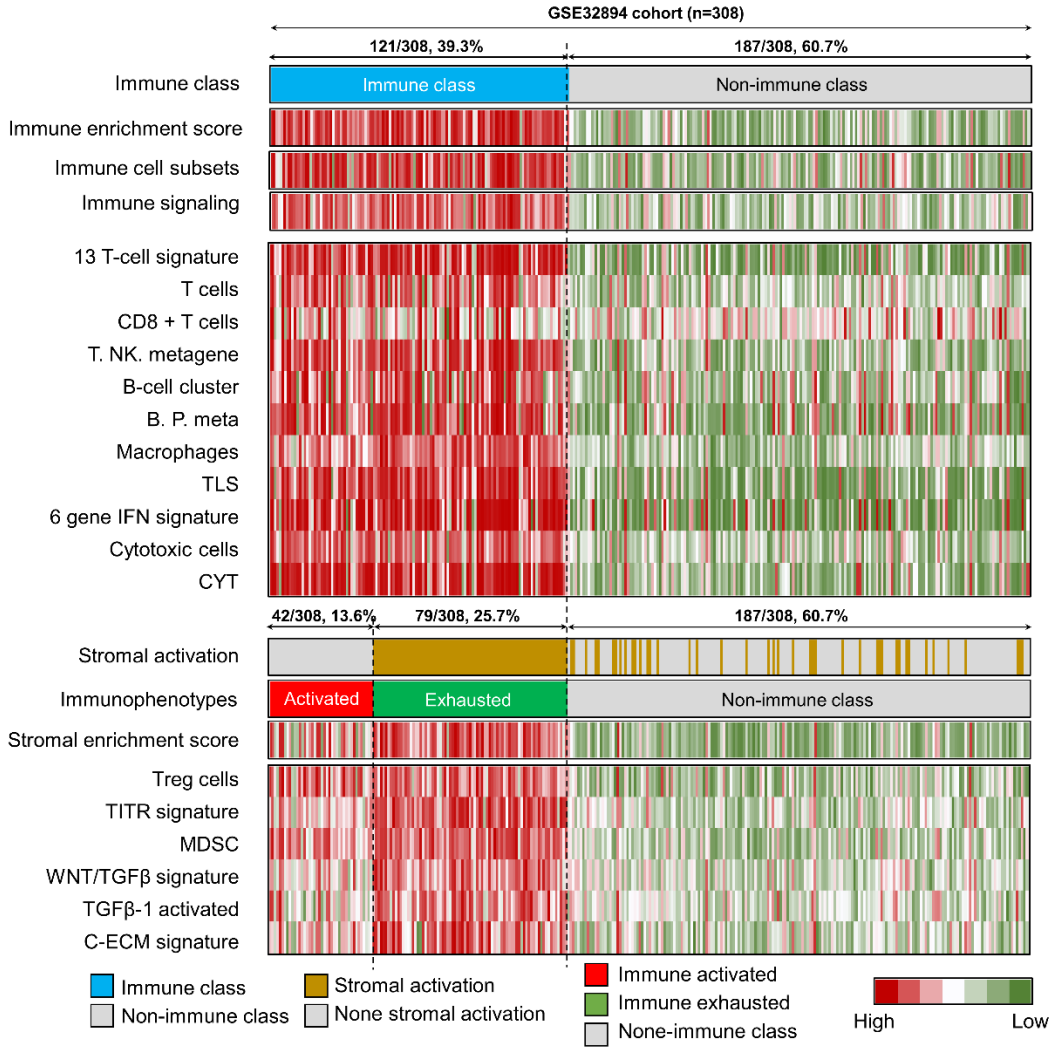

Figure 6

806

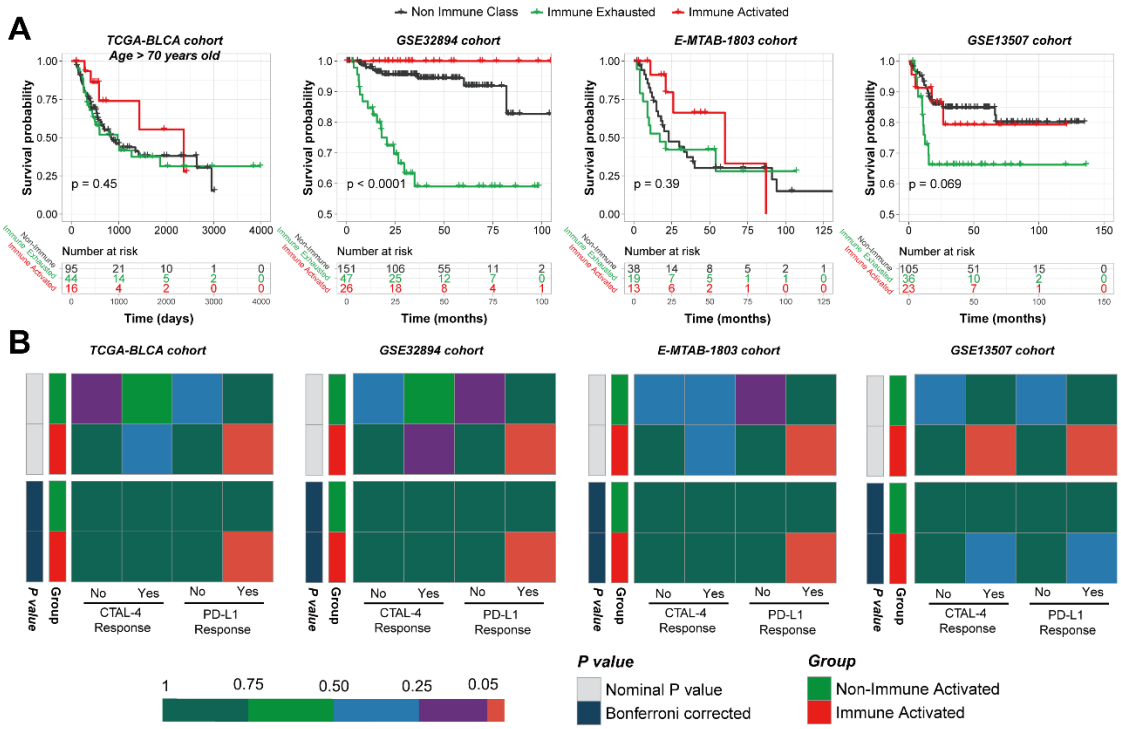

Figure 7

807

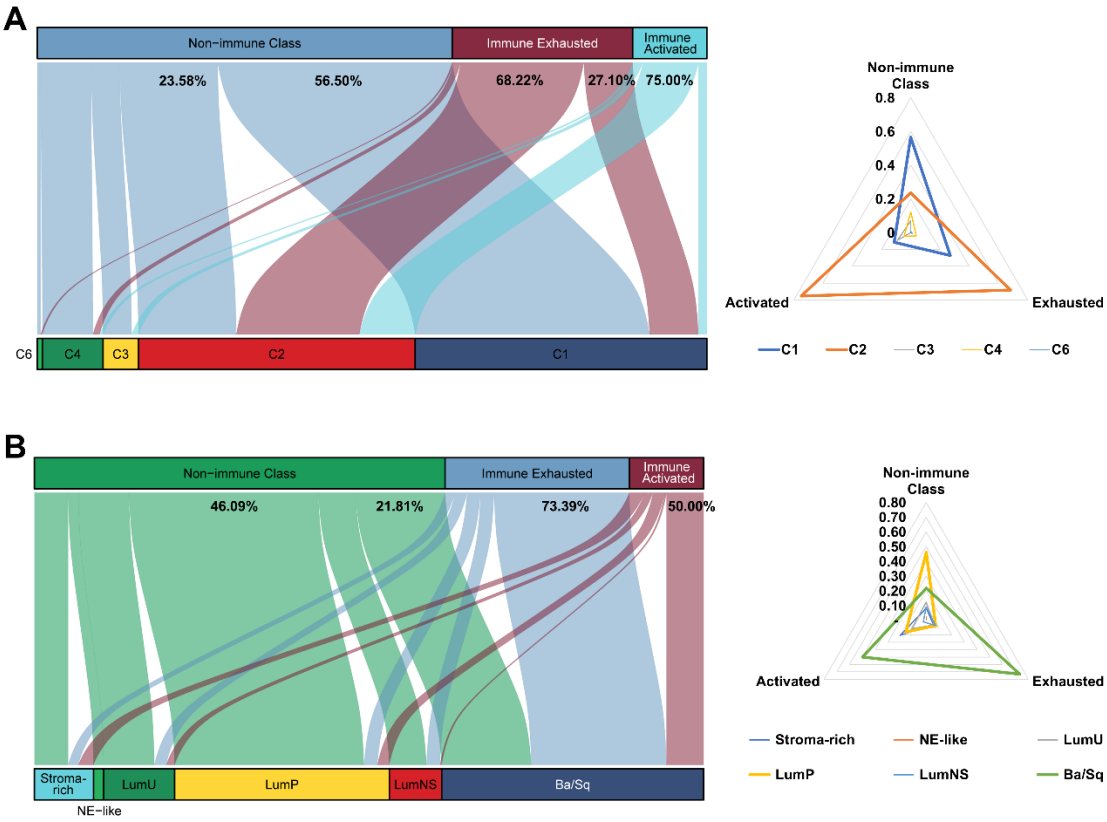

Figure 8

808